Distribution of $r \cdot p$ in Atomic Systems

Yves A. Bernard, Deborah L. Crittenden, and Peter M. W. Gill*

Research School of Chemistry, Australian National University, Canberra ACT 0200, Australia

Received: August 13, 2010; Revised Manuscript Received: September 22, 2010

We present formulas for computing the probability distribution of the posmom $s = r \cdot p$ in atoms, when the electronic wave function is expanded in a single particle Gaussian basis. We study the posmom density, $S(s)$, for the electrons in the ground states of 36 lightest atoms (H−Kr) and construct an empirical model for the contribution of each atomic orbital to the total $S(s)$. The posmom density provides unique insight into types of trajectories electrons may follow, complementing existing spectroscopic techniques that provide information about where electrons are (X-ray crystallography) or where they go (Compton spectroscopy). These, a priori, predictions of the quantum mechanically observable posmom density provide an challenging target for future experimental work.

Introduction

The properties of a quantum mechanical system of N particles are completely described[1,2] by its position wave function $\Psi(r_1, r_2, \cdots, r_N)$ or momentum wave function $\Phi(p_1, p_2, \cdots, p_N)$. However, to extract physical insight from these, one must usually construct the associated probability densities,

$$\rho(r) = N \int \cdots \int \Psi^*(r, r_2, r_3, \cdots, r_N)\Psi(r, r_2, r_3, \cdots, r_N) dr_2 \, dr_3 \cdots \, dr_N \tag{1}$$

$$\Pi(p) = N \int \cdots \int \Phi^*(p, p_2, p_3, \cdots, p_N)\Phi(p, p_2, p_3, \cdots, p_N) dp_2 \, dp_3 \cdots \, dp_N \tag{2}$$

Although the wave functions contain the same information, the densities shed different and complementary light on the behavior of matter.[3,4]

From the position and the momentum, one can construct a variety of dynamical variables. Among these, the angular momentum

$$L = r \times p \tag{3}$$

is a particularly important quantum mechanical observable. Orbital angular momentum is quantized to integer multiples of $\hbar$ and spin angular momentum to half-integer multiples, as first measured by Stern and Gerlach.[5] The development of angular momentum theory led, for example, to an understanding of nuclear magnetism[6] and the Zeeman effect.[2]

Recently, we have become interested in a fourth dynamical variable, the posmom[7−9]

$$s = r \cdot p \tag{4}$$

which is a known quantum mechanical observable.[8,9] We discovered that its density $S(s)$ is the Fourier transform of a particular autocorrelation function of the wave function, and we exploited this to obtain the exact posmom densities of a number of model systems.[8] Subsequently, by examining the H atom and LiH molecule, we showed that $S(s)$ yields insight into the nature of electronic trajectories, and we argued that electron posmometry could provide information that is invisible in position or momentum spectroscopies.[9]

When a electron follows a circular trajectory, its r and p vectors are orthogonal and its posmom s therefore vanishes. At the other extreme, along highly eccentric elliptical trajectories, r and p are almost parallel (or antiparallel) and s is large. Thus, whereas $\rho(r)$ reveals where the electrons *are*, and $\Pi(p)$ tells us where they are *going*, $S(s)$ informs us about *types of trajectories* that they follow.

In this article, we extend our investigation to (nonrelativistic) many-electron systems and study $S(s)$ for the first 36 atoms in the periodic table. We review posmom theory and derive formulas for relevant integrals over Gaussian basis functions before discussing exact results for hydrogenic ions. After presenting basis set details, we discuss atomic posmom densities $S(s)$ and their atomic orbital contributions $S_{nl}(s)$. We then propose an empirical model for the $S_{nl}(s)$ and we examine the effects of basis set and electron correlation on $S(s)$, comparing these with the corresponding effects on the spherically averaged position and momentum densities. Atomic units are used throughout.

Theory

The Fourier Transform

$$\hat{S}(k) = \int_{-\infty}^{\infty} S(s)e^{-iks} \, ds \tag{5}$$

of the posmom density can be obtained[8,9] from the hyperbolic autocorrelation

$$\hat{S}(k) = \int \rho_1(e^{+k/2}r, e^{-k/2}r) dr \tag{6}$$

* To whom correspondence should be addressed E-mail: peter.gill@anu.edu.au.

Distribution of $\boldsymbol{r} \cdot \boldsymbol{p}$ in Atomic Systems

J. Phys. Chem. A, Vol. 114, No. 44, 2010 **11985**

where ρ_1 is the spinless first-order reduced density matrix.[10] If the wave function is expanded in a basis of one-electron functions $\phi_a(\boldsymbol{r})$, one has

$$\rho_1(\boldsymbol{r}, \boldsymbol{r}') = \sum_{ab} P_{ab} \phi_a(\boldsymbol{r}) \phi_b(\boldsymbol{r}') \qquad (7)$$

where P_{ab} is a one-particle density matrix element and thus

$$\hat{S}(k) = \sum_{ab} P_{ab} [ab]_{\hat{S}} \qquad (8)$$

where the hyperbolic autocorrelation integral $[ab]_{\hat{S}}$ depends explicitly on k and is

$$[ab]_{\hat{S}} = \int \phi_a^*(\mathrm{e}^{+k/2}\boldsymbol{r}) \phi_b(\mathrm{e}^{-k/2}\boldsymbol{r}) \mathrm{d}\boldsymbol{r} \qquad (9)$$

If ϕ_a and ϕ_b are concentric unnormalized Cartesian Gaussian functions

$$\phi_a(\boldsymbol{r}) = x^{a_x} y^{a_y} z^{a_z} \mathrm{e}^{-\alpha r^2} \qquad (10a)$$

$$\phi_b(\boldsymbol{r}) = x^{b_x} y^{b_y} z^{b_z} \mathrm{e}^{-\beta r^2} \qquad (10b)$$

the integral factorizes into x, y, and z parts and vanishes unless $a_x + b_x$, $a_y + b_y$, and $a_z + b_z$ are even. In the nonvanishing case, it is given by

$$[ab]_{\hat{S}} =$$
$$\frac{\Gamma[(a_x + b_x + 1)/2]\Gamma[(a_y + b_y + 1)/2]\Gamma[(a_z + b_z + 1)/2]}{(\alpha\mathrm{e}^k + \beta\mathrm{e}^{-k})^{(l_a+l_b+3)/2}} \mathrm{e}^{(l_a - l_b)k/2}$$
$$(11)$$

where Γ is the Gamma function,[11] $l_a = a_x + a_y + a_z$, and $l_b = b_x + b_y + b_z$. The nonconcentric case is similar and is discussed elsewhere.[12] If ϕ_a and ϕ_b are s-type functions (not to be confused with the posmom symbol s), we obtain

$$[ss]_{\hat{S}} = \left(\frac{\pi}{\alpha\mathrm{e}^k + \beta\mathrm{e}^{-k}}\right)^{3/2} \qquad (12)$$

By taking the inverse Fourier transforms of eq 8 and eq 11, we obtain

$$S(s) = \sum_{ab} P_{ab} [ab]_S \qquad (13)$$

where the posmom integral $[ab]_S$ depends explicitly on s and is

$$[ab]_S =$$
$$\frac{\Gamma[(a_x + b_x + 1)/2]\Gamma[(a_y + b_y + 1)/2] \, \Gamma[(a_z + b_z + 1)/2]}{4\pi\Gamma[(l_a + l_b + 3)/2]}$$
$$\times \frac{\Gamma[(2l_a + 3)/4 - is/2]\Gamma[(2l_b + 3)/4 + is/2]}{\alpha^{(2l_a+3)/4-is/2} \beta^{(2l_b+3)/4+is/2}}$$
$$(14)$$

For two concentric s-type Gaussians, the posmom integral reduces to

$$[ss]_S = \frac{|\Gamma(3/4 + is/2)|^2}{2\alpha^{3/4-is/2}\beta^{3/4+is/2}} \qquad (15)$$

In general, $[ab]_S$ integrals are complex and have the properties $[aa]_S \in \mathbb{R}$ and $[ab]_S = [ba]_S^*$. Thus, only their real parts are important because their imaginary parts cancel in the sum eq 13.

Within a single-determinant model such as unrestricted Hartree−Fock (UHF), the density matrix P_{ab} is a sum of contributions from each of the N orbitals and we can therefore write

$$S(s) = \sum_{ab} \sum_{j=1}^{N} C_{aj}^* C_{bj} [ab]_S = \sum_{j=1}^{N} S_j(s) \qquad (16)$$

where

$$S_j(s) = \sum_{ab} C_{aj}^* C_{bj} [ab]_S \qquad (17)$$

and the C_{aj} are molecular orbital coefficients and $S_j(s)$ are the molecular orbital posmom densities. In the same way, $\hat{S}(k) = \sum_{j=1}^{N} \hat{S}_j(k)$.

The posmom density $S(s)$ is an even function, so we need consider only $s \geq 0$. The total posmom densities $S(s)$ are normalized to the total number of electrons, N, and the orbital densities $S_j(s)$ are normalized to 1, that is, $S(s) \in L^1(\mathbb{R})$. Similarly, the hyperbolic autocorrelation $\hat{S}(k)$ is an even function, so we consider only $k \geq 0$ and normalization implies $\hat{S}(0) = N$ and $\hat{S}_j(0) = 1$.

As only atomic systems will be considered in subsequent analysis and discussion, we designate a general atomic orbital posmom density by $S_{nl}(s)$, where n and l are the principal and the azimuthal quantum numbers, respectively. Upon assigning specific values to n and l, we switch to the corresponding spectroscopic symbols, that is, $1s$ ($n = 1$, $l = 0$), $2s$ ($n = 2$, $l = 0$), $2p$ ($n = 2$, $l = 1$), etc. Similar notation applies for $\hat{S}_j(k)$. We will use an overbar to designate a *per electron* quantity so, for example, the reduced posmom density $\bar{S}(s)$ is the posmom density per electron.

Hydrogenic Ions

Because the wave functions of the hydrogenic ions (i.e., H, He$^+$, ...) differ only by a dilation factor, their hyperbolic autocorrelations are identical. Moreover, they are independent of the magnetic quantum number m_l and are given by[8]

$$\hat{S}_{nl,\mathrm{H}}(k) = \mathrm{sech}^{2l+3}(k/2) P_{n-l-1}^{(0,2l+1)}(2\mathrm{sech}^2(k/2) - 1) \qquad (18)$$

where $P_n^{(a,b)}$ is a Jacobi polynomial.[11] In general, $\hat{S}_{nl,\mathrm{H}}(k)$ equals 1 at $k = 0$, possesses $n - l - 1$ roots and finally decays as $\mathrm{e}^{-(l+3/2)k}$.

The corresponding posmom densities are given by[9]

$$S_{nl,H}(s) = \frac{(-1)^{n-l-1}(n+l)!}{(n-l-1)!(2l+1)!} \frac{\left|\Gamma\!\left(l+\frac{3}{2}+is\right)\right|^2}{\Gamma\!\left(\frac{1}{2}\right)\Gamma\!\left(l+\frac{3}{2}\right)\Gamma(l+2)}$$

$$\times\; {}_4F_3\left[\begin{array}{cccc} -(n-l-1) & n+l+1 & l+\frac{3}{2}+is & l+\frac{3}{2}-is \\[2mm] l+\frac{3}{2} & l+2 & 2l+2 \end{array};1\right]$$

(19)

where ${}_4F_3$ is a hypergeometric function.[13] Although this expression is complicated, it reduces in all cases to sech πs multiplied by a polynomial in s^2. For example,

$$S_{1s,H}(s) = \frac{1}{2}(4s^2 + 1)\text{sech }\pi s \qquad (20a)$$

$$S_{2s,H}(s) = \frac{1}{8}(4s^2 + 1)^2\text{sech }\pi s \qquad (20b)$$

$$S_{2p,H}(s) = \frac{1}{24}(4s^2 + 1)(4s^2 + 9)\text{sech }\pi s \qquad (20c)$$

Figure 1 reveals that these densities vary substantially, and the number of extrema (other than at the origin) is equal to the number ($N_{node} = n - l - 1$) of radial nodes in the wave function.

The $S_{1s,H}(s)$, $S_{2p,H}(s)$ and $S_{3d,H}(s)$ densities have $N_{node} = 0$ and decrease monotonically from a maximum at $s = 0$. The $S_{2s,H}(s)$ and $S_{3p,H}(s)$ densities ($N_{node} = 1$) have a local minimum at $s = 0$ and a maximum at $s \approx 1.0$ and $s \approx 1.5$, respectively. Finally, $S_{3s,H}(s)$ ($N_{node} = 2$) has a local maximum at $s = 0$, a local minimum at $s \approx 0.7$, and a maximum at $s \approx 1.9$. For a given number of nodes, $S_{nl,H}(s)$ broadens as n and l increase, implying that large values of s (i.e., eccentric electron trajectories) are more probable for electrons in highly excited states.

Computational details

We have implemented the calculation of hyperbolic autocorrelation integrals eq 11 and posmom integrals eq 14 for Gaussian basis sets containing up to f functions in a development version of the Q-Chem quantum chemistry package.[14] Because the $[ab]_S$ integrals are available in closed form, the CPU time to compute a single value of $S(s)$ is negligible compared with the cost of the prerequisite self-consistent field (SCF) calculation.

We have computed the UHF posmom densities of all the atoms up to Kr using even-tempered Gaussian basis sets with the exponents in Table 1. The B_1 basis was used for the atoms H–Ar, and the B_2 basis for the atoms K–Kr. These sets are sufficiently large that the addition of further functions produces maximum fluctuations of less than 10^{-6} in $S(s)$ and changes of less than 10^{-7} E_h in the UHF energy.

We have also computed the MP2[15] and CCSD[16] posmom densities for H–Ar using the B_1^* basis set. This basis is sufficiently large that additional functions produce maximum fluctuations of less than 10^{-5} in the CCSD posmom density and changes of less than 1 mE_h in the MP2 or CCSD energies.

Atomic Orbital Posmom Densities

Figure 2 shows the reduced CCSD/B_1^* posmom densities $\bar{S}(s)$ of the first 10 atoms. Each curve decreases monotonically with increasing s but, because of the 2s and 2p contributions, the
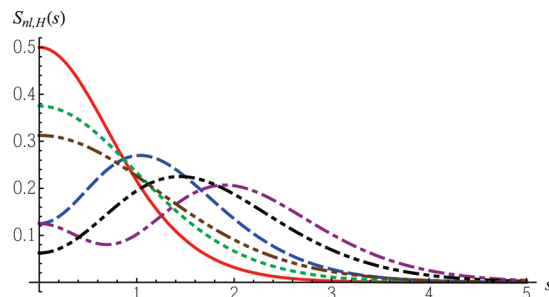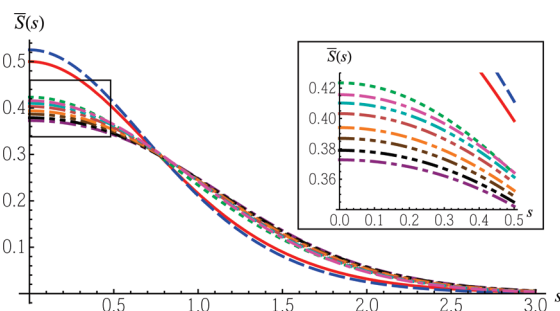

Figure 1. Posmom density $S_{nl,H}(s)$ of the hydrogenic orbital nl. 1s (solid), 2s (dash), 2p (dot), 3s (dash-dot), 3p (dash-dot-dot), 3d (dash-dot-dot-dot).

TABLE 1: Exponents of the Even-Tempered Basis Sets[a]

	B_1 and B_1^* bases	B_2 basis
s	$2^{-15}, 2^{-14}, \cdots, 2^{26}$	$2^{-20}, 2^{-19}, \cdots, 2^{35}$
p	$2^{-13}, 2^{-12}, \cdots, 2^{15}$	$2^{-18}, 2^{-17}, \cdots, 2^{23}$
d	$2^{-4}, 2^{-3}, \cdots, 2^8$	$2^{-13}, 2^{-12}, \cdots, 2^{15}$
f	$2^{-2}, 2^{-1}, \cdots, 2^5$	

[a] The d and f functions are excluded from the B_1 basis.

Figure 2. Reduced CCSD/B_1^* posmom densities $\bar{S}(s)$ in (from top to bottom) He, H, Li, Ne, F, O, N, C, B, and Be.

densities of Li–Ne are broader than those of H and He. We will discuss the trends in the origin values $\bar{S}(0)$ in the section after next.

Figure 3 shows the orbital densities $S_{nl}(s)$ for the Ne and Ar atoms. It is initially surprising that these are similar to their hydrogenic counterparts, even though the nuclear charges in Ne ($Z = 10$) and Ar ($Z = 18$) are much greater than 1. The reason, however, is straightforward: increasing Z leads to a contraction in position space and a dilation in momentum space but, to the extent that these effects are exactly matched, the posmom is rigorously invariant.[8]

Why, then, are the Ne and Ar posmom densities not identical to their hydrogenic analogs? It is because electron–electron repulsion leads not only to dilation of the orbitals in many-electron atoms but, also, to small changes in their *shapes*. Because these subtle effects are often chemically important, it is valuable to examine the difference densities

$$\Delta S_{nl,A}(s) = S_{nl,A}(s) - S_{nl,H}(s) \qquad (21)$$

that they create.

Figure 4a shows the difference densities $\Delta S_{1s,A}(s)$ for several He-like ions. In each case, the density for $s \lesssim 0.8$ is increased at the expense of larger values, indicating that electron repulsion reduces the ellipticity of the electrons' orbits. This interesting effect diminishes as Z grows (and the electron–electron repulsion becomes increasingly dominated by the nucleus-
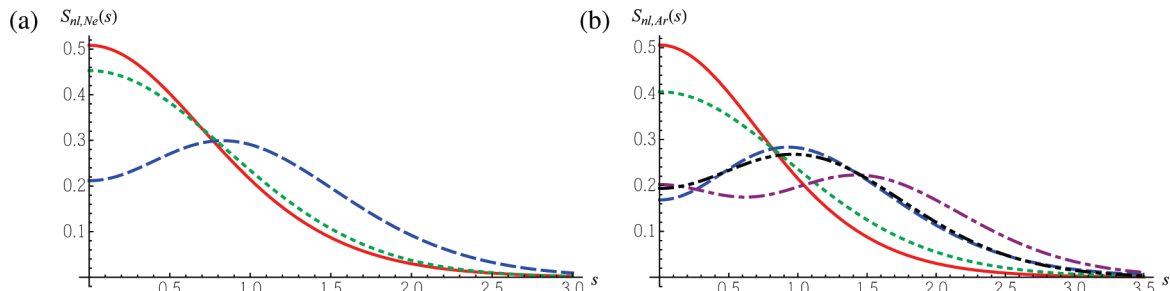
Figure 3. UHF/B$_1$ orbital densities $S_{nl}(s)$ in the Ne (a) and Ar (b) atoms. 1s (solid), 2s (dash), 2p (dot), 3s (dash-dot), 3p (dash-dot-dot).
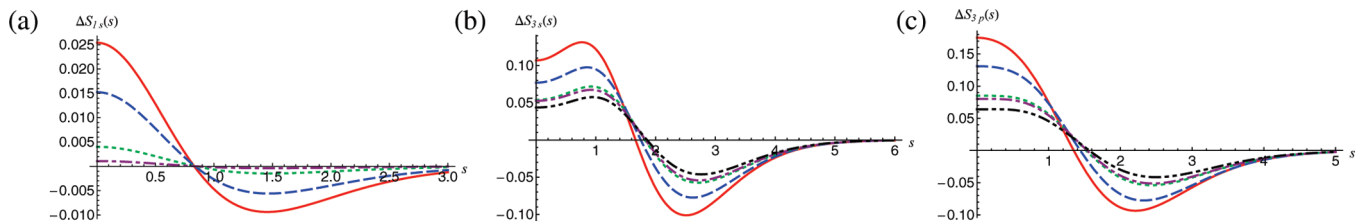
Figure 4. (a) UHF/B$_1$ difference densities $\Delta S_{1s}(s)$ in (from top to bottom) He, Li$^+$, Ne^{8+}, and Kr^{34+}. (b) UHF/B$_1$ difference densities $\Delta S_{3s}(s)$ in (from top to bottom) Al, Ar, Mn, Ga, and Kr. (c) UHF/B$_1$ difference densities $\Delta S_{3p}(s)$ in (from top to bottom) Al, Ar, Mn, Ga, and Kr.

electron attraction), and the posmom density of Kr^{34+} is very similar to that of the hydrogenic 1s orbital.

The difference densities are usually larger for the higher orbitals and, to illustrate this, Figure 4, panels b and c, shows $\Delta S_{3s,\,A}(s)$ and $\Delta S_{3p,\,A}(s)$ in the Al, Ar, Mn, Ga, and Kr atoms. Both difference densities behave qualitatively in same way as $\Delta S_{1s}(s)$, that is, the probability of small s values increases. However, the quantitative effects are much stronger: the origin value $S_{3s,\,Al}(0)$ is roughly twice as large as $S_{3s,\,H}(0)$ and, even more impressive, $S_{3p,\,Al}(0)$ is roughly four times as large as $S_{3p,\,H}(0)$. As in the He-like ions, the difference densities become smaller as Z increases. Other orbitals behave similarly.

A Model for Atomic Orbital Posmom Densities

In this section, we propose an empirical model that approximates $S_{nl}(s)$ for each orbital in the ground states of H–Kr. Inspired by the results of the foregoing section, our model begins with the hydrogenic density and corrects this for the effects of nuclear charge and other electrons in the same shell. For brevity, the model is presented in Fourier space, but all of the formulas can be transformed into real space using the two relations

$$\mathcal{F}^{-1}[k^2\hat{f}(k)] = -\frac{d^2}{ds^2}f(s) \qquad (22)$$

$$\mathcal{F}^{-1}[\text{sech}^p\,k] = \frac{2^p}{4\pi\Gamma(p)}\left|\Gamma\!\left(\frac{p+is}{2}\right)\right|^2 \qquad (23)$$

where $\mathcal{F}^{-1}$ is the inverse Fourier transform.

The difference density in Fourier space is

$$\Delta\hat{S}_{nl,A}(k) = \hat{S}_{nl,A}(k) - \hat{S}_{nl,H}(k) \qquad (24)$$

and, because of normalization, $\Delta\hat{S}_{nl,A}(0) = 0$ for any atom A. We have observed that, apart from this root at the origin, $\Delta\hat{S}_{nl,A}(k)$ always has the same number of roots as $\hat{S}_{nl,H}(k)$, and we therefore conjecture that $\Delta\hat{S}_{nl,A}(k)$ can be modeled by a polynomial

$$\Delta\hat{S}_{nl,A}^{M}(k) = k^2\sum_{i=1}^{n-l}\beta_{nl,i}\,\text{sech}^{2l+2i+1}(\alpha_{nl}k/2) \qquad (25)$$

inspired by eq 18. The k^2 factor is included to give the correct behavior near the origin, α_{nl} is a dilation/contraction factor which shifts the roots and $\beta_{nl,\,i}$ are the polynomial coefficients. After analyzing α_{nl} and $\beta_{nl,\,i}$ for all the orbitals in He–Kr, we have found that they can be approximated by

$$\alpha_{nl} = Z_{\text{eff}}^{-1}(aN^{1/3}N_{\text{sh}} + b) + c \qquad (26)$$

$$\beta_{nl,i} = Z_{\text{eff}}^{-1}(aN^{1/3}N_{\text{sh}} + b) \qquad (27)$$

where Z_{eff}^{-1} is the effective nuclear charge[17] and N_{sh} is the number of electrons in the shell of the atomic orbital nl. The parameters a, b, and c, which are collected in Table 2, were determined by least-squares fitting of the model to the UHF $S_{nl,\,A}(s)$ for each atomic orbital nl and atom A. In the optimization of $\beta_{1s,\,1}$, the constraint $a + b = 0$ was applied to ensure that $\Delta\hat{S}_{1s,H}^{M}(k) = 0$. In order to capture the behavior of the difficult $S_{4s}(s)$ orbital, we used

$$\beta_{4s,i} = Z_{\text{eff}}^{-1}(aN^{1/3}N_{\text{sh}} + b) + c \quad \text{for } i = 3, 4 \qquad (28)$$

The physical interpretation of eqs 26 and 27 is as follows:
(1) As Figure 4a shows, $\Delta S_{nl}(s)$ is inversely proportional to the nuclear charge.
(2) Because of inner-electron shielding, the relevant nuclear charge is Z_{eff}.
(3) The N_{sh} electrons in the same shell as atomic orbital nl affect α_{nl} and $\beta_{nl,\,i}$ additively.

For example, using our model, the posmom density of the carbon 2s orbital is the hydrogenic density eq 20b plus the inverse Fourier transform of the correction term eq 25, that is,

$$S_{2s,C}^{M}(s) = S_{2s,H}(s) + \mathcal{F}^{-1}[\beta_{2s,1}k^2\text{sech}^3(\alpha_{2s}k/2) +$$
$$\beta_{2s,2}k^2\text{sech}^5(\alpha_{2s}k/2)] \qquad (29)$$

TABLE 2: Optimized Values of a, b, and c for Use in Eqs 26 and 27

	α_{nl}			$\beta_{nl,1}$		$\beta_{nl,2}$		$\beta_{nl,3}$			$\beta_{nl,4}$		
nl	a	b	c	a	b	a	b	a	b	c^a	a	b	c^a
$1s$	0.5824	−1.3583	1.1045	0.0455	−0.0455								
$2s$	0.0102	−0.0735	1.0687	−0.0266	0.0108	0.1490	0.3166						
$3s$	0.0016	−0.2042	1.0255	0.0286	0.0661	−0.3706	−2.5816	0.6045	5.3900				
$4s$	−0.0064	−0.1117	0.9716	−0.0381	0.0028	0.8770	3.8958	−2.2900	−12.5871	−4.3999	1.2020	8.3560	7.9026
$2p$	−0.0578	−0.0552	1.1878	0.0702	0.0483								
$3p$	−0.0101	−0.3260	1.0524	−0.1489	−0.6774	0.3725	2.8699						
$4p$	−0.1450	−2.7142	1.7124	0.2548	1.5220	−1.4734	−17.1994	1.6191	25.4413				
$3d$	−0.0177	0.1554	1.0221	0.0868	−0.8868								

^{a} The $\beta_{4s,3}$ and $\beta_{4s,4}$ coefficients are given by eq 28.
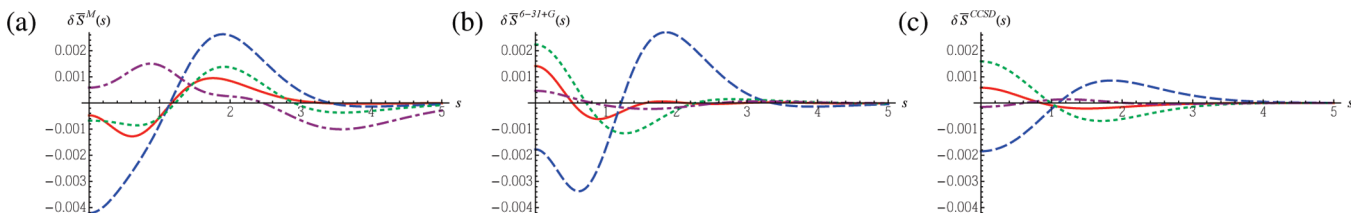
Figure 5. (a) Model errors, (b) 6-31+G basis holes, and (c) CCSD correlation holes for He (solid), Be (dash), Ne (dot), and Ar (dot-dash).

where, using $Z_{\text{eff}} = 3.25$, $N = 6$, $N_{sh} = 4$, and the parameters in Table 2,

$$\alpha_{2s} = 3.25^{-1}(+0.0102 \times 6^{1/3} \times 4 - 0.0735) + 1.0687 = \\ +1.0689 \quad (30a)$$

$$\beta_{2s,1} = 3.25^{-1}(-0.0266 \times 6^{1/3} \times 4 + 0.0108) = -0.0562 \quad (30b)$$

$$\beta_{2s,2} = 3.25^{-1}(+0.1490 \times 6^{1/3} \times 4 + 0.3166) = +0.4306 \quad (30c)$$

Figure 5a shows the reduced model error

$$\delta\bar{S}^{M}(s) = \bar{S}^{M}(s) - \bar{S}^{UHF}(s) \quad (31)$$

for the He, Be, Ne, and Ar atoms. Of these, Be has the largest maximum error (≈ -0.004), and this represents a relative error of roughly 1%. The integrated model error

$$\bar{\varepsilon}_{S}^{M} = \int_{0}^{\infty} |\delta\bar{S}^{M}(s)| \, ds \quad (32)$$

is given for all atoms up to Kr in Table 3. For H−Ar, the mean $\bar{\varepsilon}_{S}^{M}$ value is 0.00295; over all of the atoms, it is 0.00266. The maximum error, $\bar{\varepsilon}_{S}^{M} = 0.00629$, arises for the Be atom.

The Special Value $s = 0$

The electron density at the nucleus and the momentum density at the origin are important quantities. The first, $\rho(0)$, arises in the expectation value of the Darwin term[18] of the nonrelativistic limit of the hydrogen Dirac equation[19] and in the Fermi contact term[20] used in electron paramagnetic resonance (EPR) spectroscopy.[21] It can be measured experimentally or determined by standard ab initio methods.[22,23] The second, $\Pi(0)$, appears in the Maclaurin expansion of the spherically averaged momentum density[24] and can be obtained from high-energy electron impact experiments[25] or ab initio calculations.[26,27]

The origin posmom density $S(0)$ is also important, for it directly measures the probability of circular electronic trajectories.[9] For example, as we saw earlier, Figure 4a shows that the electrons' orbits are more circular in the He atom than in the H atom.

The origin density $S_{nl,H}(0)$ of a hydrogenic ion is[9]

$$S_{nl,H}(0) = \frac{1}{n\pi}\left[\frac{\Gamma\left(\frac{n-l+1}{2}\right)\Gamma\left(\frac{n+l+1}{2}\right)}{\Gamma\left(\frac{n-l}{2}\right)\Gamma\left(\frac{n+l+2}{2}\right)}\right]^{\gamma} \quad (33)$$

where $\gamma = (-1)^{n-l}$, and this is given in Table 4 for various orbitals. The highest values arise for orbitals with no radial nodes ($N_{\text{node}} = 0$) and the maximum, $S_{1s,H}(0) = 1/2$, arises in the lowest orbital. For a fixed value of N_{node}, the origin density decreases as n grows.

Table 5 lists the reduced origin posmom densities $\bar{S}(0)$ for the atoms H−Kr at the UHF level. The average value across a

TABLE 3: Integrated Model Error × 1000 for H−Kr

	$\bar{\varepsilon}_{S}^{M}$		$\bar{\varepsilon}_{S}^{M}$		$\bar{\varepsilon}_{S}^{M}$
H	0.00	Al	1.98	Mn	1.75
He	1.50	Si	1.84	Fe	1.82
Li	3.65	P	2.36	Co	2.06
Be	6.29	S	2.03	Ni	2.31
B	4.89	Cl	2.65	Cu	4.17
C	4.07	Ar	3.66	Zn	2.64
N	2.79	K	2.26	Ga	1.56
O	4.11	Ca	3.67	Ge	1.61
F	3.88	Sc	2.68	As	1.59
Ne	2.77	Ti	2.24	Se	2.22
Na	1.82	V	1.99	Br	2.14
Mg	2.74	Cr	4.63	Kr	1.54

TABLE 4: Origin Posmom Densities of Hydrogenic Orbitals

$N_{\text{node}} = 0$		$N_{\text{node}} = 1$		$N_{\text{node}} = 2$		$N_{\text{node}} = 3$	
nl	$S_{nl,H}(0)$	nl	$S_{nl,H}(0)$	nl	$S_{nl,H}(0)$	nl	$S_{nl,H}(0)$
$1s$	0.5	$2s$	0.125	$3s$	0.125	$4s$	0.07031
$2p$	0.375	$3p$	0.0625	$4p$	0.11719	$5p$	0.04688
$3d$	0.3125	$4d$	0.03906	$5d$	0.10938	$6d$	0.03418

Distribution of $r \cdot p$ in Atomic Systems

J. Phys. Chem. A, Vol. 114, No. 44, 2010 **11989**

TABLE 5: Reduced UHF Origin Posmom Densities $\bar{S}(0)$ and Model Errors $\delta\bar{S}^M(0)$ for H–Kr

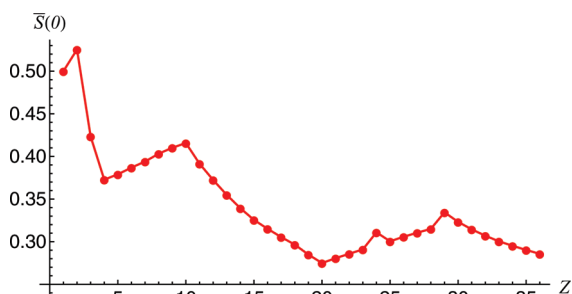|	$\bar{S}(0)$	$\delta\bar{S}^M(0)$		$\bar{S}(0)$	$\delta\bar{S}^M(0)$		$\delta\bar{S}(0)$	$\bar{S}^M(0)$
H	0.50000	0.00000	Al	0.35491	0.00026	Mn	0.30048	0.00011
He	0.52541	−0.00047	Si	0.33928	0.00081	Fe	0.3058	−0.00077
Li	0.42347	0.00315	P	0.32554	0.00142	Co	0.31055	−0.00123
Be	0.37278	−0.00422	S	0.31513	0.00045	Ni	0.31506	−0.00160
B	0.37904	−0.00341	Cl	0.30543	0.00028	Cu	0.33444	−0.00204
C	0.38692	−0.00261	Ar	0.29655	0.00058	Zn	0.32325	−0.00197
N	0.39401	−0.00121	K	0.28492	0.00111	Ga	0.31447	−0.00086
O	0.40320	−0.00245	Ca	0.27495	0.00093	Ge	0.30700	−0.00034
F	0.41018	−0.00205	Sc	0.28065	0.00050	As	0.30044	−0.00000
Ne	0.41569	−0.00068	Ti	0.28583	0.00041	Se	0.29520	−0.00032
Na	0.39152	0.00102	V	0.29095	0.00024	Br	0.29031	−0.00038
Mg	0.37245	−0.00047	Cr	0.31097	0.00214	Kr	0.28575	−0.00026

row of the periodic table decreases from 0.51270 (He row), to 0.39816 (Ne row), to 0.33760 (Ar row), to 0.30061 (Kr row). The maximum density (0.52541) occurs for He and the minimum (0.27495) for Ca. The trends in the $\bar{S}(0)$ values, shown in Figure 6, can be understood qualitatively by referring to the hydrogenic values in Table 4. For example, the fact that $S_{1s,\,H}(0) > S_{2p,\,H}(0) > S_{2s,\,H}(0)$ explains why $\bar{S}(0)$ falls from He to Be, but then rises from Be to Ne. Similar arguments apply to the heavier atoms.

The reduced origin model errors are also given in Table 5 and the largest (0.0042) occurs for Be. The mean absolute error for H–Ar is 0.0014, and this drops to 0.0011 for H–Kr.

Basis Effect on $S(s)$

We have studied the sensitivity of $S(s)$ to basis set by comparing the standard Pople basis sets B = STO-3G, 6-31G, 6-31+G, 6-311G or 6-311+G with the B_1 basis. The reduced posmom basis holes

Figure 6. Reduced UHF origin posmom densities $\bar{S}(0)$ for H–Kr.

$$\delta\bar{S}^B(s) = \bar{S}^B(s) - \bar{S}^{B_1}(s) \tag{34}$$

for He, Be, Ne, and Ar using the B = 6-31+G basis are plotted in Figure 5b. The biggest hole arises for Be, where the 6-31+G basis underestimates $S(s)$ for small and large s and overestimates it for midrange s. The errors are smaller and in the opposite direction for He, Ne, and Ar.

To assess the basis set quality over all values of s, we define the integrated basis error

$$\bar{\varepsilon}_S^B = \int_0^\infty |\bar{S}^B(s) - \bar{S}^{B_1}(s)|\, ds \tag{35}$$

and compare it with its position and momentum analogs

$$\bar{\varepsilon}_\rho^B = \int_0^\infty |\bar{\rho}^B(r) - \bar{\rho}^{B_1}(r)|4\pi r^2\, dr \tag{36}$$

$$\bar{\varepsilon}_\Pi^B = \int_0^\infty |\bar{\Pi}^B(p) - \bar{\Pi}^{B_1}(p)|4\pi p^2\, dp \tag{37}$$

where $\rho(r)$ and $\Pi(p)$ are the spherically averaged position and momentum densities[28]

$$\rho(r) = \frac{1}{4\pi} \int \rho(\mathbf{r})\, d\Omega_r \tag{38}$$

$$\Pi(p) = \frac{1}{4\pi} \int \Pi(\mathbf{p})\, d\Omega_p \tag{39}$$

The errors, eqs 35–37, were calculated for H–Ar and are presented in Table 6. As anticipated, all the errors decrease with increasing basis size but we find that $S(s)$ shows the least sensitivity to basis set and $\Pi(p)$ the most. For $S(s)$, the addition of diffuse functions is particularly important; for $\rho(r)$, adding extra functions to the valence shell is more effective; $\Pi(p)$ benefits equally from both, but still has a larger overall error than either $S(s)$ or $\rho(r)$. To achieve the same accuracy as $\rho(r)$ and $\Pi(p)$ with the 6-311G basis, one needs only the 6-31G basis for $S(s)$. (For some systems, 6-311G is worse than 6-31G. and it has been observed[29] that 6-311G is not of triple-ζ quality.)

TABLE 6: Integrated Basis Errors ×1000 for H–Ar

	$\bar{\varepsilon}_S^B$					$\bar{\varepsilon}_\rho^B$					$\bar{\varepsilon}_\Pi^B$				
	STO-3G	6-31G	6-31+G	6-311G	6-311+G	STO-3G	6-31G	6-31+G	6-311G	6-311+G	STO-3G	6-31G	6-31+G	6-311G	6-311+G
H	7.7	16.05	3.90	2.77	0.97	284.5	25.5	29.11	4.14	4.33	305.6	74.4	30.1	12.7	9.63
He	31.7	9.75	0.97	4.43	0.92	72.7	13.58	14.55	5.98	6.32	94.4	40.25	22.97	19.78	13.28
Li	18.5	5.38	2.94	0.52	0.61	127.8	13.22	8.54	6.23	6.21	127.8	28.28	17.28	3.67	3.56
Be	30.2	14.49	6.08	3.23	0.17	148.9	28.81	10.18	5.63	4.45	163.9	57.97	22.44	10.9	3.8
B	35.7	16.57	3.59	4.27	0.98	180.8	26.1	8.47	4.39	5.86	183.3	50.53	17.53	13.74	9.87
C	37.2	12.86	0.70	4.71	1.07	121.2	16.78	8.06	4.82	6.19	131.6	31.58	7.78	16.35	12.39
N	41.2	6.75	2.06	5.10	1.44	91.2	9.98	10.21	5.19	6.44	101.0	23.8	19.17	19.01	15.04
O	50.6	8.41	2.76	6.37	2.05	111.6	11.42	10.97	6.88	7.93	128.4	26.4	22.37	21.59	18.31
F	57.7	11.63	2.30	7.23	2.37	124.5	11.52	11.12	7.61	8.97	144.7	32.54	21.75	23.94	20.64
Ne	63.7	12.76	2.32	7.86	2.41	137.6	12.47	12.25	8.25	9.67	163.4	35.68	23.2	26.12	22.03
Na	28.7	0.43	0.25	0.63	0.49	143.4	3.49	3.63	5.98	5.95	133.3	7.91	7.41	5.26	4.61
Mg	34.4	0.96	0.14	0.64	0.26	158.3	2.33	2.05	2.96	2.98	159.4	6.06	3.82	4.96	3.91
Al	35.6	1.28	0.79	1.03	0.57	150.1	2.19	2.31	1.69	1.79	146.5	5.64	5.46	5.39	4.51
Si	34.0	1.68	0.52	1.43	0.51	122.7	2.04	2.33	1.51	1.63	125.2	6.45	5.05	6.11	4.36
P	33.6	1.65	0.27	3.32	1.86	107.1	2.02	2.08	6.88	4.21	112.8	5.82	4.15	17.92	13.79
S	34.9	1.88	0.37	2.63	1.50	97.2	2.13	2.07	4.94	3.02	106.7	6.63	4.96	14.59	10.73
Cl	29.3	2.12	0.44	2.27	1.84	79.9	2.22	2.41	5.35	3.60	69.8	7.04	5.35	15.50	13.54
Ar	32.3	2.45	0.56	1.68	0.48	81.6	2.43	2.65	1.93	1.93	77.8	7.80	5.94	6.29	4.64
Mean	35.4	7.06	1.72	3.34	1.14	130.0	10.46	7.94	5.02	5.08	137.5	25.27	13.71	13.55	10.48

TABLE 7: Origin Reduced Posmom Correlation Holes ×1000 for H−Ar

	$\delta\bar{S}^{MP2}(0)$	$\delta\bar{S}^{CCSD}(0)$		$\delta\bar{S}^{MP2}(0)$	$\delta\bar{S}^{CCSD}(0)$
H	0.00	0.00	Ne	1.06	1.59
He	−1.04	0.58	Na	0.21	0.72
Li	−0.71	−0.12	Mg	−1.12	−0.12
Be	−1.37	−1.85	Al	−0.89	−0.24
B	−0.54	−0.62	Si	−0.78	−0.29
C	−0.22	0.14	P	−0.63	−0.27
N	−0.01	0.62	S	−0.41	−0.25
O	0.50	1.16	Cl	−0.21	−0.21
F	0.83	1.44	Ar	−0.01	−0.15

TABLE 8: Integrated Correlation Errors ×1000 for H−Ar

	$\bar{\varepsilon}_S^C$		$\bar{\varepsilon}_\rho^C$		$\bar{\varepsilon}_\Pi^C$	
	MP2	CCSD	MP2	CCSD	MP2	CCSD
H	0.00	0.00	0.00	0.00	0.00	0.00
He	1.13	0.58	3.04	1.47	6.08	1.67
Li	0.65	0.17	5.07	2.73	4.91	2.24
Be	3.53	2.55	14.72	12.43	29.38	14.18
B	1.75	0.78	7.4	6.49	14.51	5.77
C	1.06	0.23	5.00	3.42	7.95	1.65
N	0.66	0.84	5.19	2.40	5.04	1.62
O	0.78	1.46	8.17	3.16	9.25	3.75
F	1.08	1.77	10.31	3.68	12.6	4.92
Ne	1.31	1.91	11.57	3.95	14.48	5.46
Na	0.32	0.83	11.06	4.53	11.46	4.77
Mg	2.10	0.51	12.13	6.09	17.14	6.75
Al	1.56	0.48	8.59	4.88	11.41	4.66
Si	1.36	0.44	6.79	4.02	10.10	3.69
P	1.20	0.35	5.62	3.34	9.73	3.04
S	1.03	0.29	4.86	2.96	8.11	2.28
Cl	0.90	0.24	4.57	2.58	8.04	1.93
Ar	0.80	0.24	4.48	2.26	8.27	1.72
Mean	1.18	0.76	7.14	3.91	10.47	3.89

Correlation Effect on $S(s)$

The reduced posmom correlation hole is defined as the difference

$$\delta\bar{S}^C(s) = \bar{S}^C(s) - \bar{S}^{UHF}(s) \qquad (40)$$

between the correlated and UHF reduced posmom densities, where C is CCSD or MP2. Reduced CCSD posmom holes for He, Be, Ne, and Ar are shown in Figure 5c, and the MP2 and CCSD origin reduced holes for H−Ar in Table 7.

The origin posmom correlation hole $\delta\bar{S}^C(0)$ increases monotonically from a negative value in Be to a positive value in Ne. Physically, this means that correlation causes the electron trajectories in Be to become less circular, but those in Ne to become more so, and this can probably be traced to the $2s/2p$ near-degeneracy static correlation[30] in Be, B, and C, which is replaced by primarily dynamic correlation in the heavier atoms. The holes in other atoms lie between these two extremes and, although the MP2 and CCSD origin holes are broadly similar, there are some cases (notably He and C) where they have opposite signs.

Overall, correlation effects are small for $S(s)$ and, to compare them with $\rho(r)$ and $\Pi(p)$, we define the integrated correlation errors

$$\bar{\varepsilon}_S^C = \int_0^\infty |\bar{S}^C(s) - \bar{S}^{UHF}(s)|\, ds \qquad (41)$$

and report these in Table 8.

$$\bar{\varepsilon}_\rho^C = \int_0^\infty |\bar{\rho}^C(r) - \bar{\rho}^{UHF}(r)|4\pi r^2\, dr \qquad (42)$$

$$\bar{\varepsilon}_\Pi^C = \int_0^\infty |\bar{\Pi}^C(p) - \bar{\Pi}^{UHF}(p)|4\pi p^2\, dp \qquad (43)$$

For all three densities, the Group II metals exhibit the largest correlation effects, showing again the consequences of strong static correlation in these small-gap atoms. Overall, $\Pi(p)$ is most strongly affected by correlation, followed by $\rho(r)$ and then $S(s)$. Compared with CCSD, MP2 tends to overcorrelate by a factor of about 2. This is consistent with previous results.[28,31]

Conclusions

In this article, we have presented formulas for the integrals required to calculate atomic posmom densities $S(s)$ from wave functions using Gaussian basis functions. We have used these to compute posmom densities for the first 36 atoms in the periodic table (H−Kr) and proposed an empirical scheme that models orbital contributions to the total posmom density via corrections to the contributions of the corresponding hydrogenic orbitals.

The error of the model is comparable to the 6-31+G basis error and the MP2 correlation error. The largest model errors, basis set errors and correlation errors arise for the Be atom. We have also found that $S(s)$ is more robust than either $\rho(r)$ or $\Pi(p)$ to basis set and correlation effects and we attribute this to cancelation effects between the position and momentum components of s. We conclude that the UHF/6-31+G level of theory provides a good approximation to the exact $S(s)$ for atoms.

The next step in this investigation is the extension to molecular systems, where we anticipate that polarization functions will play a larger role. We are currently undertaking such a study and will report our results elsewhere.[12]

References and Notes

(1) Cohen-Tannoudji, C.; Diu, B.; Laloe, F. *Quantum Mechanics*, 2nd ed.; Wiley: New York, 1977; Vol. 1.
(2) Cohen-Tannoudji, C.; Diu, B.; Laloe, F. *Quantum Mechanics*, 2nd ed.; Wiley: New York, 1977; Vol. 2.
(3) Sands, D. E. *Introduction to Crystallography*; Benjamin: New York, 1969.
(4) Weigold, E.; McCarthy, I. E. *Electron Momentum Spectroscopy*; Kluwer: New York, 1999.
(5) Gerlach, W.; Stern, O. *Z. Phys.* **1922**, *9*, 353–355.
(6) Abragam, A. *Principles of Nuclear Magnetism*; Oxford University Press: 1983.
(7) Twamley, J.; Milburn, G. J. *New J. Phys.* **2006**, *8*, 328.
(8) Bernard, Y. A.; Gill, P. M. W. *New J. Phys.* **2009**, *11*, 0830185.
(9) Bernard, Y. A.; Gill, P. M. W. *J. Phys. Chem. Lett.* **2010**, *1*, 1254–1258.
(10) Davidson, E. R. *Reduced Density Matrices in Quantum Chemistry*; Academic: New York, 1976.
(11) *NIST Handbook of Mathematical Functions*; Olver, F. W. J., Lozier, D. W., Boisvert, R. F., Clark, C. W., Eds.; Cambridge University Press: New York, 2010.
(12) Bernard, Y. A.; Crittenden, D. L.; Gill, P. M. W. in preparation.
(13) Slater, L. J. *Generalized Hypergeometric Functions*; Cambridge University Press: Cambridge, England, 2008.
(14) Shao, Y.; et al. *Phys. Chem. Chem. Phys.* **2006**, *8*, 3172–3191.
(15) Møller, C.; Plesset, M. S. *Phys. Rev.* **1934**, *46*, 618–622.
(16) Purvis, G. D.; Bartlett, R. J. *J. Chem. Phys.* **1982**, *76*, 1910–1918.
(17) Slater, J. C. *Phys. Rev.* **1930**, *36*, 57–64.
(18) Darwin, C. G. *Proc. R. Soc. Lond. A* **1925**, *115*, 654–680.
(19) Dirac, P. A. M. *Proc. Roy. Soc. (London)* **1928**, *117*, 610–624.
(20) Fermi, E. *Z. Phys.* **1930**, *60*, 320–333.

Distribution of $\boldsymbol{r} \cdot \boldsymbol{p}$ in Atomic Systems

J. Phys. Chem. A, Vol. 114, No. 44, 2010 **11991**

(21) Wertz, J. E.; Bolton, J. R. *Electron Spin Resonance: Elementary Theory and Practical Applications*; McGraw-Hill: New York, 1972.

(22) Batra, R.; Bernd, G.; Spichty, M.; Gescheidt, G.; Houk, K. N. *J. Chem. Phys.* **1996**, *100*, 18371–18379.

(23) Hermosilla, L.; Calle, P.; de la Vega, J. M. G.; Sieiro, C. *J. Phys. Chem. A* **2005**, *109*, 1114–1124.

(24) Thakkar, A. J. *J. Chem. Phys.* **1987**, *86*, 5060–5062.

(25) Bonham, R. A.; Wellenstein, H. F. *Compton Scattering: The Investigation of Electron Momentum Distributions*; McGraw-Hill: New York, 1977; pp 234–272.

(26) Thakkar, A. J. *Adv. Chem. Phys.* **2004**, *128*, 303–352.

(27) Roy, A. K.; Thakkar, A. J. *Chem. Phys. Lett.* **2002**, *362*, 428–434.

(28) Crittenden, D. L.; Bernard, Y. A. *J. Chem. Phys.* **2009**, *131*, 054110.

(29) Grev, R. S.; Schacfer, H. F. III *J. Chem. Phys.* **1989**, *91*, 7305–7306.

(30) Linderberg, J.; Shull, H. *J. Mol. Spectrosc.* **1960**, *5*, 1–16.

(31) Meyer, H.; Muller, T.; Schweig, A. *J. Mol. Struct. (Theochem)* **1996**, *360*, 55–65.